Analysis of the Thermal Conductivity of Epoxy and Reaction Bonded Silicon Nitride Matrix Particulate Composites

by Clifford Stephens

Submitted to the Department of Materials Science and Engineering in partial fulfillment of the requirements for the Degree of

Bachelor of Science

at the

Massachusetts Institute of Technology

February, 1996

Signature of Author . . . . . .
Department of Materials Science and Engineering
January 19, 1996

Certified by . . . . Jan. 22, 1996
Professor Yet-Ming Chiang
Thesis Supervisor

Certified by 1/19/96
Dr. John Haggerty
Thesis Supervisor

Accepted by . . .
Professor David K.Roylance
Chairman, Undergraduate Thesis Committee

Analysis of the Thermal Conductivity of Epoxy and Reaction Bonded Silicon Nitride Matrix Particulate Composites

by Clifford Stephens

Submitted to the Department of Materials Science and Engineering
on January 19, 1996 in partial fulfillment of the requirements
for the Degree of Bachelor of Science in Materials Science and Engineering

ABSTRACT

The feasibility of creating high thermal conductivity RBSN matrix particulate composites was studied using various high thermal conductivity filler materials. First, epoxy matrix particulate composite samples with particles of differing filler materials were created by colloidal pressing. The relative thermal conductivity, or ratio of the composite thermal conductivity to the matrix thermal conductivity (K_C/K_M) for the hexagonal boron nitride (HBN) and chemical vapor deposition grade diamond (CVD-D) samples were found to be 268 and 88, respectively. These experimental values were much higher than theoretical predictions (expected value was $\approx$10 for Bruggeman model). Next, reaction bonded silicon nitride (RBSN) matrix particulate composite samples with filler particles of HBN and CVD-D were colloidally pressed. The RBSN matrix composite samples had lower than expected relative thermal conductivities (all under 1). The good performance of the epoxy-HBN and epoxy-diamond samples relative to theoretical models has been attributed to a particle percolation. On the other hand, the low thermal conductivities of the RBSN matrix samples were attributed to microcracks which caused poor mechanical contact between the RBSN matrix and filler particles. The microcracks formed during cooling after nitridation and were caused by thermal expansion coefficient mismatch between the matrix and filler materials. If high thermal conductivity RBSN matrix particulate composites are to be developed, a high thermal conductivity filler material with a similar thermal expansion coefficient must be employed.

Thesis Supervisors: Professor Yet-Ming Chiang, Department of Materials Science and Engineering

Dr. John Haggerty, Senior Research Scientist, Department of Materials Science and Engineering

TABLE OF CONTENTS

	page
Title Page	1
Abstract	2
Table of Contents	3
List of Figures and Illustrations	5
List of Tables and Graphs	6
Introduction	7
Overview	7
Applications of research	7
Production process/properties of RBSN	8
Background theory/mathematical models for solid-state heat transport	9
Types of carriers in solid-state heat transport	9
Thermal conductivity in metals	9
Thermal conductivity in non-metallic crystals	9
Origins of thermal boundary resistance	10
Definition of thermal boundary resistance	10
Mathematical models of boundary resistance	11
The acoustic mismatch model	12
The diffuse mismatch model	14
Quantitative comparison of the models	14
The Kapitza radius	15
Thermal conductivity of particulate composites	16
The Maxwell model	18
The Bruggeman model	18
The effect of porosity on thermal conductivity	19
Experimental Procedure	20
Epoxy matrix sample preparation	20
Description of colloidal pressing	20
Thermal diffusivity measurements	21
Epoxy matrix composite samples	22
RBSN matrix composite samples	23

TABLE OF CONTENTS (continued)

	page
Results and discussion	24
Epoxy matrix samples	24
RBSN matrix samples	25
Future RBSN research	27
Conclusion	38
References	39

LIST OF FIGURES AND ILLUSTRATIONS

		page
Figure #1:	Plot of R_{BD} ratio vs. dissimilarity for mismatch models	15
Figure #2:	Relative thermal conductivity vs. volume fraction for Maxwell and Bruggeman models	17
Figure #3:	Epoxy matrix sample data vs. Bruggeman and Maxwell models	29
Figure #4:	Schematic of die apparatus of a colloidal press	21
Figure #5:	Schematic of thermal diffusivity measurement apparatus	22
Figure #6:	SEM micrographs of HBN-epoxy composite sample	30
Figure #7:	R_{BD} vs. filler shear modulus and density for epoxy	36
Figure #8:	R_{BD} vs. filler shear modulus and density for RBSN	37

LIST OF TABLES

		page
Table #1:	Boundary resistance calculations for epoxy samples	31
Table #2:	Relative thermal conductivity and Kapitza radius calculations for epoxy samples	32
Table #3:	Boundary resistance calculations for RBSN samples	33
Table #4:	Relative thermal conductivity and Kapitza radius calculations for RBSN samples	34
Table #5:	Percent conversion and volume fraction calculations for RBSN samples	35

INTRODUCTION

Overview. The ultimate objective of this study was to assess the feasibility of creating RBSN matrix composite samples with high thermal conductivities (defined here as 30 W/m·°K or greater) using various filler materials including aluminum nitride (AlN), cubic boron nitride (CBN), hexagonal boron nitride (HBN), and diamond. Although pure RBSN has a thermal conductivity of approximately 7 W/m·°K, its mechanical and thermal properties may be considerably improved by composite development involving the addition of dispersed particles of high thermal conductivity material. However, since most prior art and mathematical models concerning phonon heat transport in composite materials deal with zero porosity materials (and RBSN has innate porosity), a preliminary study was done using epoxy as a matrix material. Epoxy was chosen as the material of choice for the preliminary study primarily for two reasons: low cost and the fact that before curing, it flows like a low viscosity liquid. This second property was critical, given the need to produce samples with zero void space (in order to mirror the mathematical models as closely as possible). Once large boosts in thermal conductivity were achieved in epoxy matrix samples, research commenced with RBSN as a matrix material.

Applications of research. RBSN ceramic is an excellent candidate material for use in applications which require a high thermal shock resistance from high temperature fluxes and relatively low capacitance. This is due to RBSN's good mechanical properties, relatively low dielectric constant, and similar expansion coefficient with some of the base materials used in these applications. RBSN offers significant processing advantages over sintered or hot-pressed silicon nitride (Si_3N_4), the most important of which is a much lower consolidation temperature (on the order of 400 - 600°C lower than Si_3N_4) and shorter consolidation times. Despite the fact that RBSN possesses an innate residual porosity on the order of 10 - 25%, fracture strength and oxidation resistances equal or better the properties of fully-dense Si_3N_4.[1, 2] Some of the other materials being

presently used in high temperature flux applications are alumina, beryllium oxide (BeO), silicon carbide (SiC), aluminum nitride (AlN), hexagonal boron nitride (HBN), and diamond. All of these alternative materials have higher thermal conductivities than RBSN. The thermal conductivities for these competing materials range from 30 W/m·°K (alumina) to 2,000 W/m·°K (diamond). A high thermal conductivity is critical for any potential material to be considered for use in high temperature flux applications so that heat can be quickly dissipated and removed from the environment of the application.

Production process/properties of RBSN. RBSN is produced by the heating of a preformed mass of silicon under a nitriding atmosphere until all of the silicon has been converted into Si_3N_4. The silicon preform usually takes the form of a silicon powder compact generated by any one of a number of pressing schemes (colloidal pressing, etc.). The nitriding gas is normally nitrogen (N_2), a nitrogen/hydrogen (N_2/H_2) mixture, or ammonia (NH_3). The nitridation reaction causes a 22% volumetric increase in the material. Because the reaction takes place within the void space of the compacted silicon, the density of the product material increases without any shrinkage. As mentioned above, RBSN has a characteristic residual porosity level on the order of 10 - 25% because an interconnected pore structure is necessary in the nitridation stage to allow for the free transport of the nitriding gas to all parts of the compact. [1, 2]

RBSN production using ultra-high purity silicon provides three major advantages over normal Si_3N_4: high purity in the end product (which improves the thermal conductivity), shorter nitriding times, and lower processing temperatures. Sintered Si_3N_4 and conventional RBSN (using low grade silicon) processing involves heating schedules which require a temperature in excess of the melting point of silicon (1,550°C) and furnace times of up to 150 hours. However, when using high purity silicon, RBSN processes typically run at approximately 1,300°C for approximately 20 hours. Additionally, high purity end product is achieved by default due to the fact that no sintering aids or other impurities are introduced to the material during the production process. [1]

BACKGROUND THEORY AND MATHEMATICAL MODELS FOR SOLID-STATE HEAT TRANSPORT

Types of carriers in solid-state heat transport. Modern solid-state heat transport theory assumes free electrons and phonons to be the dominant carriers of thermal energy in metals and non-metallic crystals, respectively. Phonons are wavelike (mathematical) solutions which model atomic lattice vibrations and are quantized into packets of energy related to the quantum excitation level, or mode, of a given lattice vibration. The relationship between phonons and lattice vibrations in crystals is analogous to the relationship between light photons and the vibrational frequency of light waves.[3]

Thermal conductivity in metals. In the case of metals, an analogy can be easily drawn between electrical conductivity and thermal conductivity with respect to free electrons. In Drude theory of electrical conductivity, the conductivity is related to the mean free path of the electron, which is the average distance an electron will travel due to the presence of an electric field before colliding with another atom (and subsequently resume its normal, purely thermal motion). With thermal conductivity, electrons are assigned a mean free path related to the increased velocity acquired due to thermal gradients in a material before transferring the extra energy to another atom. The thermal conductivity (K) of a metal can be expressed in the following manner[4]:

$$K = \rho \cdot C \cdot \upsilon \cdot \lambda / 3 \qquad [1]$$

ρ = Density of material
C = Heat capacity of material
υ = Mean thermal velocity of free electrons in lattice
λ = Mean free path of free electrons in lattice

Thermal conductivity in non-metallic crystals. Due to the fact that atoms are closely coupled in a crystal lattice, increases in vibrational energy resulting from temperature gradients are constantly transmitted to other parts of the lattice. Debye (1914) was the originator of the concept in which heat could be transmitted by lattice vibrations in the form of waves (which in turn led to the modern theory of phonons). In

Debye's model, the mean free path is considered to be equal to the distance these waves are able to travel before their intensity is attenuated by scattering to 1/e of its initial value. In modern theory, the mean free path is a measure of the rate at which energy is exchanged between different phonon modes. Thus, an expression similar to equation [1] can be used to describe the thermal conductivity of non-metallic crystals, but with υ being represented by the Debye velocity of the material. The Debye velocity of a material is closely related to its acoustic properties (ie. how quickly a sound wave propagates through the lattice) and can be calculated by[4]:

$$\upsilon = (G / \rho)^{0.5} \qquad [2]$$

G = Shear modulus of material

As a general rule, non-metallic crystals with high thermal conductivities will tend to have the following four traits: low atomic mass, strong interatomic bonding, simple crystal structure, and low anharmonicity.[3]

Origins of thermal boundary resistance. The subject of measuring the thermal boundary resistance between two materials has been closely studied by several people during the 20th century. The first research concerning thermal boundary resistances was carried out by Kapitza in 1941. Kapitza's research concentrated on metal-liquid helium interfaces at extremely low temperatures (below 1°K). These liquid-solid interfaces, called Kapitza boundaries, have become the basis for modelling thermal boundary resistances in modern solid-state heat transport theory. However, unlike solid-liquid Kapitza interfaces, which one can automatically assume to have perfect mechanical and chemical contact, solid-solid interfaces have boundaries and other imperfections (ie. microcracks, etc.) which cause relatively poor adherance leading to scattering in thermal carriers (and an accompanying loss of thermal conductivity across the interface).[5]

Definition of thermal boundary resistance. The specific (thermal) boundary resistance (sometimes referred to as the Kapitza resistance) across a solid-solid interface (R_{BD}) can be defined by the following equation:

$$R_{BD} = \Delta T / Q \qquad [3]$$

ΔT = Temperature discontinuity across interface
Q = Heat flux across interface

The thermal boundary resistance is a function of the number of incident phonons on a given interface, the energy of each phonon, and the probability that a given phonon will be transmitted across the boundary. Whereas with the thermal conductivity of a material, the most difficult parameter to calculate is the carrier mean free path, the phonon transmission probability is the most difficult (and most critical) parameter to determine for the thermal boundary resistance.[5]

Mathematical models of boundary resistance. Two widely accepted theoretical models exist to explain thermal boundary resistance: the acoustic mismatch model (Mazo and Onsager, 1955)[6] and the diffuse mismatch model (Swartz, 1986).[7] The acoustic mismatch model is considered to be an upper limit of the boundary resistance, while the diffuse mismatch model is a lower limit. The two models are very similar and many of the fundamental assumptions made by each model are common to each other. Both models operate under the assumption that thermal transport across a boundary is due exclusively to phonons. Also, all phonons incident upon a boundary have only two distinct possibilities: (1) they can be transmitted across the boundary, or (2) not. The transmission probability is a function of the phonon mode, wave vector, and frequency. Although the transmission probability does have some temperature dependence, this factor is not taken into account by either model. This last assumption is significant because it allows one to discount the presence of other phonons on the transmission probability of a given phonon. Next, all anharmonic interactions are discounted which implies that the transmission probabilities need only be calculated for one side. Finally, the principle of detailed balance is used. The principle of detailed balance states that in thermal equilibrium, the number of phonons in a given state (in terms of polarization and wave vector) leaving one side of an interface is equal to the number of phonons in an identical state returning from the other side. In order to find the net heat flow at a boundary, one need only calculate the gross heat transfer from one side of the boundary at

the two incident phonon temperatures. The net heat flow is simply the difference between these two gross heat transfer quantities. Equation [3] results from a generalization of these concepts.[5]

The acoustic mismatch model. The critical simplifying assumption made by the acoustic mismatch model is that phonons are subject to continuum acoustics and that the boundary interface is modeled as a plane. In other words, phonons are to be treated as plane waves and phonon wave propagation occurs in space, as opposed to being restricted to a lattice. Since most phonons have wavelengths much greater than typical interatomic spacings, this assumption is generally considered to be a safe one. More importantly, the model restricts incident phonons to four "options" when encountering a boundary: specular reflection, reflection plus mode conversion, refraction, and refraction plus mode conversion. Each of these four probabilities, in addition to the angles of reflection and refraction, can be calculated by invoking the acoustic analog of Snell's Law for electromagnetic waves:

$$\sin \theta_{tran} = (\upsilon_1 / \upsilon_2) \cdot \sin \theta_{in} \qquad [4]$$

θ_{tran} = Angle of phonon transmission
θ_{in} = Angle of incidence
υ_x = Phonon (Debye) velocity in material x

The above equation implies that for each pair of materials, a critical "cone" (or set of angles less than the critical angle) exists which an incident phonon must lie within in order to have any chance of being transmitted across the boundary. For solid-solid interfaces, critical angles can be relatively large and a significant fraction of incoming phonons have no chance of being transmitted. The fraction of all incoming diffuse phonons which have any chance of being transmitted (q) can be calculated from the ratio of the Debye velocities of the two materials:

$$q = 0.5 \cdot (\upsilon_1 / \upsilon_2)^2 = 0.5 \cdot \sin^2 \theta_C \qquad [5]$$

θ_C = Critical angle between material 1 and material 2

The continuum acoustics assumption allows for the transmission probabilities to be calculated from the acoustic analog of the Fresnel equations. These relationships can be derived using the following boundary conditions: (1) the normal and tangential components of displacement are continuous at the interface and (2) the "normal component" of the stress tensor is a vector that is the continuous force across the surface of the interface. It should be noted that these boundary conditions ignore the possibility of any elastic or inelastic scattering. The mathematical proofs for this quantitative analysis are given by Auld (1973).[8] In simple terms, these boundary conditions imply that if the force acting on the boundary is not continuous, then the interface (which in itself has zero mass) would be subject to infinite acceleration (which cannot and does not occur).

The Fresnel equations can be simplified by modelling transmission probabilities in terms of an acoustic impedance since phonons are conducted in a manner similar to sound waves. For the acoustic mismatch model, the impedance (Z) is represented by:

$$Z = \rho \cdot \upsilon \qquad [6]$$

This allows the transmission probability of a phonon (p) to be expressed in a manner similar to the formula for transmission at transmission line junction:

$$p = 4 \cdot Z_1 \cdot Z_2 / (Z_1 + Z_2)^2 \qquad [7]$$

Thus, an averaged transmission probability for an individual incident phonon (η) would be given by:

$$\eta = p \cdot q \qquad [8]$$

Finally, the thermal boundary resistance can be approximated by way of a Debye model[5]:

$$R_{BD} = 4 / (\rho \cdot C \cdot \upsilon \cdot \eta) \qquad [9]$$

The diffuse mismatch model. The most important assumption made by the acoustic mismatch model is that no scattering occurs at the boundary. The diffuse mismatch model takes the opposite extreme and assumes that all phonons are diffusely scattered when encountering an interface. This major assumption is why the diffuse model sets an upper limit to the effect that diffuse scattering can have on phonon conduction. The model also assumes that acoustic correlations at interfaces are completely destroyed by the diffuse scattering. In other words, a scattered phonon does not "remember" where it came from. Thus, the only determinants of the transmission probability are densities of phonon states (by way of Fermi's rule) and the principle of detailed balance because the probability that a phonon is transmitted is independent of its origins.

The quantitative analysis of the diffuse mismatch model is identical to that of the acoustic mismatch model in all regards save one: the calculation of the phonon transmission probabilities. The diffuse scattering assumption is defined by declaring that the transmission probability for a phonon from material 1 to material 2 is independent of its incoming wave vector and mode. Thus, the probability of reflection from one side must equal the probability of transmission from the other. Given this fact, the transmission probabilities can be expressed in terms of phonon velocities and phonon densities of state. Furthermore, the Debye approximation of the transmission probabilities yields a ratio of the Debye velocities. This implies that the transmission probabilities differ from the acoustic mismatch model by a density factor.[5]

Quantitative comparison of the models. Figure #1[5] shows the quantitative differences in the acoustic mismatch and diffuse mismatch models relative to dissimilarity in the two materials at the interface. The dissimilarity parameter is a ratio of the densities and Debye velocities of the two materials. As one can see, for most solid-solid interfaces, the difference in the models is on the order of ±30%. Additionally, Weis and Swartz[9] have demonstrated that solid-solid thermal boundary resistances are relatively insensitive to diffuse scattering effects (diffuse scattering is thought to be on

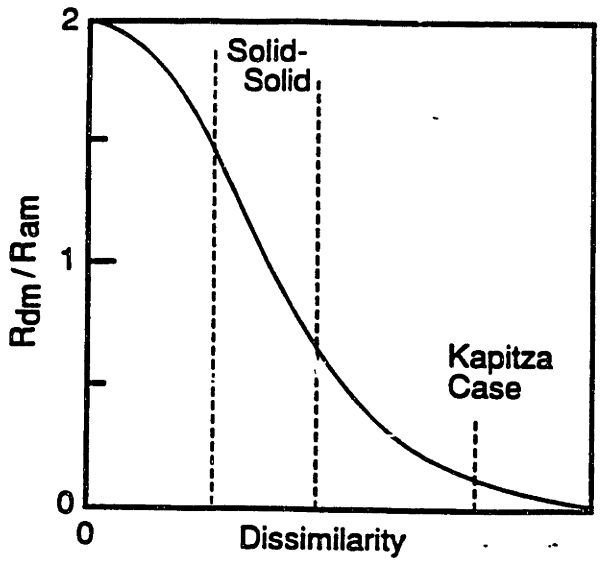

Figure #1: Plot of ratio of diffuse mismatch model R_{BD} to the acoustic mismatch mode R_{BD} vs. dissimilarity

the order of 10%). Thus, the calculations shown in this paper will work off of the acoustic mismatch model.[5]

The Kapitza radius. Now that the thermal boundary resistance of a solid-solid interface and the thermal conductivity of a material have been defined, the two must be related to one another if the thermal conductivity of composites is to be discussed. For the purposes of this paper, all composites will be assumed to be particulate composites with uniformly dispersed spherical particles of identical size surrounded by a continuous matrix. If the thermal conductivity of the filler material is much higher than the matrix material, two opposing forces, the high thermal conductivity of the filler material and the thermal boundary resistance between the filler and matrix materials, will drive the level of the composite thermal conductivity. Given the same volume fraction of filler material, larger particles (albeit fewer) will provide a smaller total boundary surface area. Thus, the thermal boundary resistance will actually be lower even with the same amount of filler material. This fact has been confirmed by Hasselman (1991).[10]

A parameter called the Kapitza radius (a_K) of a particulate composite material will now be defined to be the following:

$$a_K = R_{BD} \cdot K_M \qquad [10]$$

K_M = Thermal conductivity of matrix material

The Kapitza radius is an important parameter because it quantitatively signifies the particle size at which the effect of the higher innate thermal conductivity of the filler material is balanced by the thermal boundary resistance at the matrix-particle interfaces. If one also defines a dimensionless parameter α below as:

$$\alpha = a_K / a \qquad [11]$$

a = Radius of dispersed particles (composite filler material)

the significance of the Kapitza radius can be easily visualized. In Figure #2,[10] the ratio of the composite thermal conductivity and the matrix thermal conductivity (K_C/K_M) is plotted versus the volume fraction of spherical dispersions. When the particle size is equal to the Kapitza radius, K_C/K_M is constant with respect to volume fraction of diamond. However, when the particle sizes are larger than the Kapitza radius, the ratio increases with respect to volume fraction, and when the particle sizes are smaller, the reverse holds true. It should be noted that Hasselman (1991) has found that the conducting limit for a particulate composite at fixed volume fraction is reached when the particle size reaches approximately 10 times the size of the Kapitza radius.[10]

Thermal conductivity of particulate composites. Rayleigh and Maxwell were the first to research transport properties of composite materials. Their theories were based on obtaining temperature distributions within the composite and applying these solutions to find the effective thermal conductivity. However, their analysis focused on small volume fractions for the dispersed phase and only recently have these models been expanded to allow for larger volume fractions by Hasselman, Johnson (1985),[11] and Benveniste

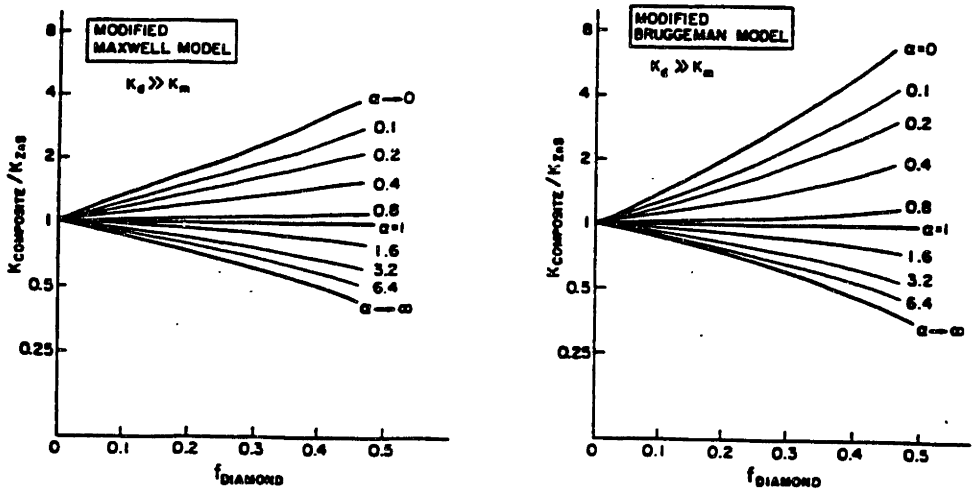

Figure #2: Relative thermal conductivity (K_C/K_M) vs. volume fraction of dispersions for Maxwell and Bruggeman models

(1986).[12] If one considers a filler material composed of particles with size a (which can be converted to α with the appropriate theoretical calculations), thermal conductivity of K_D, and occupying volume fraction f, one can derive the following equation:

$$\frac{K_C}{K_M} = \frac{[K_D \cdot (1 + 2\alpha) + 2K_M] + 2f \cdot [K_D \cdot (1 - \alpha) - K_M]}{[K_D \cdot (1 + 2\alpha) + 2K_M] - f \cdot [K_D \cdot (1 - \alpha) - K_M]} \qquad [12]$$

where the thermal conductivity of a material can be experimentally determined by using the following equation:

$$K = D \cdot C \cdot \rho \qquad [13]$$

D = Thermal diffusivity of material

If one applies the rule of mixtures, then a similar equation results for the composite thermal conductivity:[10]

$$K_C = D_C \cdot \{ (\rho_D \cdot C_D \cdot f_D) + [\rho_M \cdot C_M \cdot (1 - f_D)] \} \qquad [14]$$

The Maxwell model. This paper will provide two models for estimating the relative thermal conductivity of particulate composites: the Maxwell model and the Bruggeman model. The Maxwell model deals with low volume fractions of the dispersed phase, and this paper will assume that the model is only valid up to the 20 volume percent range. For this range of volume fractions, the model agrees very closely with the values yielded by the Bruggeman model and a plot of the two models in this range can be superimposed. In the limit of small volume fractions (ie. Maxwell model), equation [12] reduces to the following:

$$K_C / K_M = 1 + 3f \cdot [K_D \cdot (1 - \alpha) - K_M] / [K_D \cdot (1 + 2\alpha) + 2K_M] \qquad [15]$$

If the thermal conductivity of the filler material is assumed to be much greater than the matrix thermal conductivity ($K_D >> K_M$), then equation [13] reduces to:

$$K_C / K_M = [1 + 2f \cdot (1- \alpha) / (1 + 2\alpha)] / [1 - f \cdot (1 - \alpha) / (1 + 2\alpha) \qquad [16]$$

Furthermore, if $a >> a_K$ and $\alpha \rightarrow 0$, and the thermal boundary resistance becomes negligible, then equation [14] can be simplified to the following:[10]

$$K_C / K_M = 1 + 2f / (1 - f) \qquad [17]$$

The Bruggeman model. A quantitative analysis of the thermal conductivity of high volume fraction particulate composites requires a great deal of knowledge concerning the correlations between particles and their polarizations. These effects can be estimated to a degree by using Bruggeman medium theory which is based on the premise that fields of neighboring particles can be accounted for by incrementally adding the effects of each particle. At each increment, the surrounding medium can be assumed to be the existing composite at that stage (or concentration). Bruggeman theory yields the following equation after integration of the differential of equation [8] using the limits of 0 and f:

$$(1 - f)^3 = (K_M/K_C)^{(1 + 2\alpha)/(1 - \alpha)} \cdot \{ [K_C - K_D \cdot (1 - \alpha)] / [K_M - K_D \cdot (1 - \alpha)] \}^{3/(1 - \alpha)} \quad [18]$$

Once again, in the limit where $K_D >> K_M$, equation [16] reduces to:

$$K_C / K_M = [1 / (1 - f)]^{3 \cdot (1 - \alpha)/(1 + 2\alpha)} \quad [19]$$

Then, in the limit where $a >> a_K$ and $\alpha \rightarrow 0$, equation [17] becomes:

$$K_C / K_M = (1 - f)^{-3} \quad [20]$$

The Bruggeman model applies to high volume fractions. However, since the model assumes a particulate composite with dispersed filler material particles, the upper bound of the volume fraction range for which the model is valid is limited by the percolation limit of the particles. The percolation limit is the volume fraction at which all particles in a particulate composite must be contacting each other. In the case of spherical particles with cubic and hexagonal lattices, this volume fraction is on the order of 0.6 - 0.7. A plot of the theoretical relative thermal conductivity vs. particle volume fraction (both valid volume fraction ranges) for both the Bruggeman and Maxwell models is shown on Figure #3.[10]

The effect of porosity on thermal conductivity. As most ceramic materials contain some amount of innate porosity (RBSN included), this issue must be raised. Pores are known to be scattering centers for photons and even small fractions of porosity strongly reduce the photon mean free path. However, since the thermal boundary resistance models described above do not cover photon conduction, this fact will be ignored. At relatively low temperatures, voids have a low conductivity in comparison to any solid phases present and the thermal conductivity decreases linearly with the amount of void space present.[13]

EXPERIMENTAL PROCEDURE

Epoxy matrix sample preparation. During the first phase of epoxy research, an alternative sample preparation method to colloidal pressing (described below) was sought. This step was deemed necessary due to the drawbacks inherent with colloidal pressing which include long turn-around times for sample production and a general lack of control over sample volume fractions when working with a low viscosity matrix material such as epoxy. Epoxy samples were prepared by mixing the epoxy resin and curing agent by hand and introducing the mixture into a small (approximately 1 cm diameter and 0.5 cm height) cylindrical container which had hexagonal boron nitride (HBN) or aluminum nitride (AlN) particles lying at the bottom. The epoxy used for this research had a commercial name of Epothin and had a relatively low viscosity (similar to maple syrup) and density (1.13 g/cm^3). Samples were prepared in the following three ways: 1) by pipette, 2) under low pressure (0.1 atm), and 3) by pipette and later centrifuging. In each case the sample was heated for 1 hour in an oven at 80°C to accelerate the curing process of the epoxy. Unfortunately, none of the alternative methods was successful because in each case, the mixing of the resin and curing agent left behind air bubbles (leaving behind some amount of porosity) which could not be removed later. Thus, as a result of the observations made on these various processing methods, colloidal pressing became the sample preparation method of choice for this study.

Description of colloidal pressing. Colloidal pressing is a method used to produce composite samples in the form of small cylindrical pellets. Generally, the process yields samples which are relatively defect free and have a high packing density. A schematic of the die apparatus of a colloidal press is provided in Figure #4. Colloidal pressing is facilitated by a slurry which is composed of a solvent (lubricating liquid) which is mixed with the materials which will form the pellet itself. The slurry is placed between two opposing pistons in a die and a high amount of pressure (4 - 7 MPa) is applied

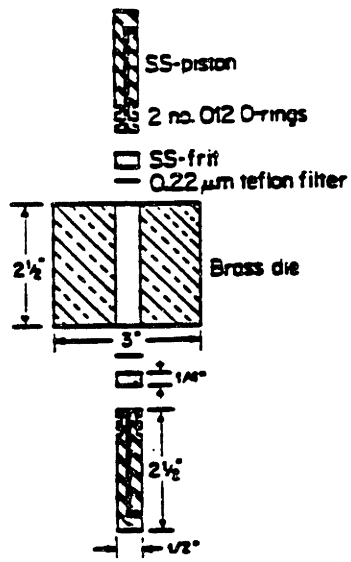

Figure #4: Schematic of die apparatus of a colloidal press

bidirectionally. The apparatus used in this research had brass pistons and a brass die. The frits were both stainless steel, with one being porous in order to allow solvent to pass through as pressure was applied on the pistons. Membrane filters were used to cover both frits in order to facilitate solvent extraction through the porous frit and to protect the sample from any impurities. Due to the size of the die used for this study, samples had a diameter of 13 mm and thicknesses ranging from 2.5 - 6 mm.

Thermal diffusivity measurements. The thermal diffusivity of each sample was measured by Prof. D. Hasselman of the Materials Science and Engineering Dept. at Virginia Polytechnic Institute. The experimental system employed was based on the pulse diffusivity method. A diagram of the apparatus used in the measurements is shown in Figure #5.[14] In this scheme, the xenon flash lamp deposits a burst of energy on the face of the sample while an infrared (IR) detector monitors the temperature on the back surface. The signal output voltage from the detector is recorded as a function of time by a PC based data acquisition system. The temperature gradient in the sample is kept below

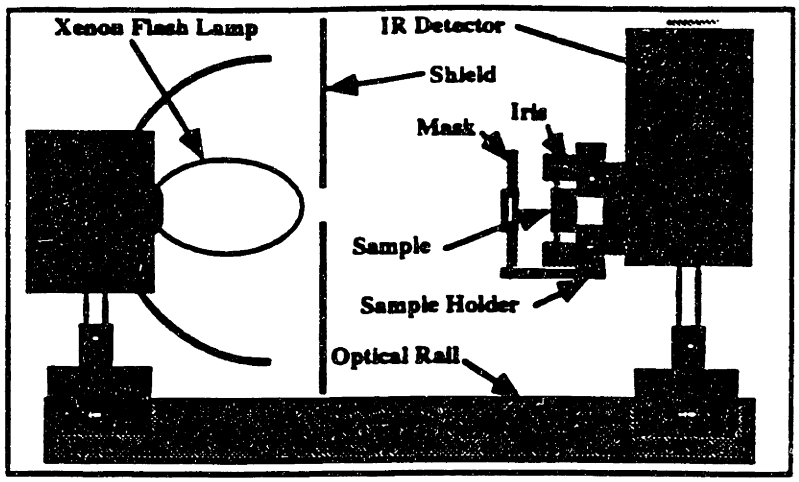

Figure #5: Schematic of thermal diffusivity measurement apparatus

2°C by periodically varying the energy being sent to the front of the sample by the xenon flash lamp. Limiting the energy deposited on the sample also prevents driving the IR detector into the nonlinear response region.

Epoxy matrix composite samples. Attempts were made to prepare one epoxy reference sample and five epoxy matrix composite samples by colloidal pressing. The filler materials used in the other five samples were the following: HBN (General Electric HPC-40 grade, 2-7 μm), cubic boron nitride (CBN) (General Electric industrial grade, 88-105 μm), chemical vapor deposition grade diamond (CVD-D) (Raytheon, 25-50 μm), abrasive grade diamond (AG-D) (General Electric, 6-12 μm), and AlN. In the case of epoxy, neither a solvent nor a binder was not used since the epoxy itself acted as a lubricant. The AlN sample was unusable because the sample was not able to maintain its shape after removal from the die due to the small grain size of the stock available. Each of the samples was heated at 80°C for 1 hour in order to accelerate curing. Due to the fact that the samples were very fragile prior to curing, the membrane filters were left attached to the samples during the curing process. The filters were later removed by polishing with 600 grit paper. The polished samples were then submitted for characterization to

Prof. Hasselman. After the samples were returned, the volumes were calculated using a water displacement method[20] and the samples were weighed. Finally, the HBN sample was viewed by scanning electron microscopy (SEM) in the axial and radial directions by Dr. Julia Sigalovsky of the Materials Processing Center (MPC) at M.I.T. to rule out the possibility of preferred orientation in the sample due to HBN's platelet macrostructure.

RBSN matrix composite samples. One pure RBSN reference sample and six RBSN matrix composite samples were prepared by colloidal pressing. Four of the six composite samples had HBN as the filler material, while the other two samples had CVD-D as the filler material. The silicon used for the samples was of ultra high purity and the stock was kept in a glove box under nitrogen. The RBSN-HBN composite samples were formulated so that the resulting samples would have filler particle volume fractions of approximately 70, 60, 50, and 30 percent after nitriding. The RBSN-diamond samples were formulated with targets of approximately 65 and 20 volume percent after nitriding. The liquid used to press the pellets was xylene and no binder was utilized. Unfortunately, the high volume fraction diamond sample was extremely brittle and crumbled while being manipulated. The remaining six samples were then nitrided by Anne-Marie Lightfoot of the M.I.T. MPC using high purity nitrogen gas at 19 kPa in a furnace according to the following specifications: (step 1) 10 minutes hold at 41°C, (2) 356 minute ramp-up (+3.40°C/min) to 1250°C, (3) 600 minute hold at 1250°C, (4) 220 minute ramp-up (+0.50°C/min) to 1360°C, (5) 240 minute hold at 1360°C, (6) 80 minute ramp-up (+0.50°C/min) to 1400°C, (7) 600 minute hold at 1400°C, (8) 390 minute ramp-down (-3.48°C/min) to 41°C. The samples were weighed before and after nitriding in order to determine the percent conversion of silicon. The thermal diffusivities were measured and then X-ray diffraction (XRD) was performed on the surface of each sample by Dr. Sigalovsky in order to determine the percent conversion of silicon and find any preferred orientations in the samples.

RESULTS AND DISCUSSION

Epoxy matrix samples. Boundary resistance calculations for the epoxy samples have been summarized in Table #1 and relative thermal conductivity and Kapitza radius calculations have been summarized in Table #2 . The densities of HBN, CBN, diamond, and epoxy were assumed to be 2300,[15] 3500,[15] 3520,[16] and 1148[17] kg/m^3, respectively. The heat capacities were assumed to be 700,[15] 700,[15] 509,[16] and 1800[17] J/kg·°K, respectively. Finally, the shear moduli were assumed to be 2.29E+10,[15] 2.29E+10,[15] 5.76E+11,[16] and 1.00E+09[18] kg/m·sec^2, respectively. Substituting parameters into equation [9] yielded boundary resistances of 1.06E-07, 8.16E-08, and 8.58E-06 K/m^2·W, for HBN, CBN, and diamond, respectively. The volume fractions of the samples were calculated using the composite mass, composite volume, and densities of the materials based on the assumption that the samples contained no porosity. The lack of porosity in the samples was ascertained by viewing a cross section of a HBN sample using optical microscopy. The diffusivities of the samples were measured to be 3.32E-05, 1.33E-06, 1.05E-05, 1.47E-06, and 1.11E-07 m^2/sec, for HBN, CBN, CVD-D, AG-D, and epoxy, respectively. The diffusivities were used to calculate the composite thermal conductivities using equation [14]. K_C was found to be 61.44, 2.97, 20.13, and 2.85 W/m·°K, for HBN, CBN, CVD-D, and AG-D, respectively. The relative thermal conductivities (K_C/K_M) were found to be, in order, 267.86, 12.96, 87.76, and 12.41. Finally, the Kapitza radii (using equation [10]) for these material combinations were all found to be smaller than 2μm.

Since the particle sizes of the filler material stock used for this study were all at least 10 times greater than the Kapitza radii, Hasselman's rule of thumb about minimizing the boundary resistance can be assumed to be in effect and equations [17] and [20] apply for modeling the above results. While the relative thermal conductivity values for CBN and AG-D agree very well with both models, the values for HBN and CVD-D exceed the expected values by an order of magnitude. The relative thermal conductivities of the epoxy matrix samples are compared with the Bruggeman and Maxwell models in Figure

#3. One explanation for the relatively high K_C/K_M value of diamond and HBN samples is that particle aggregrates formed during sample pressing because the volume fraction approaches the percolation limit and the particles were not uniformly dispersed. As stated previously, an important assumption of both the Bruggeman and Maxwell models is isotropic particle dispersion throughout the composite. The SEM micrograph of the HBN sample shown in Figure #6, which clearly demonstrates a lack of preferred orientation, lends credence to this explanation. Another possible explanation for the difference in diamond and boron nitride performance is a difference in the innate thermal conductivity of the filler materials themselves which is a function of macrostructure and impurity levels.

Unfortunately, no way exists to directly determine the thermal conductivity of the filler material itself. If one considers an "ideal" linear relationship between volume fraction and the thermal conductivity, then the HBN particles must have a thermal conductivity of at least 120 W/m·°K given the volume fraction of the HBN sample (approximately 0.5) and the thermal conductivity of epoxy (nearly 0 W/m·°K). Since the high purity HBN has a thermal conductivity of approximately 200 W/m·°K, the HBN can be assumed to have relatively low impurity levels. Thus, the thermal conductivity of the HBN sample seems to show a relatively low negative deviation from the ideal case. Conversely, the poor thermal conductivities of the diamond and CBN samples seem to indicate high levels of impurities. The results from this initial epoxy phase were encouraging and consequently, a similar study using RBSN matrix composite samples was done.

RBSN matrix samples. Identical calculations to those for epoxy were performed on the RBSN samples and have been summarized on Table #3 and Table #4. The density, heat capacity, and shear modulus of RBSN were assumed to be 2580 kg/m^3, 800 J/kg·°K, and 1.30E+11 kg/m·sec^2, respectively.[15] The boundary resistances and Kapitza radii for HBN and CVD-D were found to be 3.36E-10 and 2.16E-09 K/m^2·W, and 5.75E-09 and 3.69E-08 m, respectively. Percent conversion (for both XRD and weight difference methods) and volume fraction calculations for the RBSN samples have been summarized

on Table #5. These volume fractions, which were all close to the targeted values, have been used in the thermal conductivity calculations in Table #4. The weight difference percent conversions were rather normal and ranged from 85.4% - 100.46%, with only one sample (HBN 70%) being under 91%. The XRD percent conversions were much higher, ranging from 95.7% - 99.0%. The difference between the values of the two separate methods probably lies with the fact that XRD only measures the surface. The lower values for the weight difference method would seem to indicate that, especially in the case of high volume fraction filler samples, the nitriding gas was blocked from reaching the raw silicon in certain regions of the sample. Another explanation for this phenomenon was that impurities had been adsorbed onto the surface of the filler particles, which then evaporated during nitriding.

Unlike the epoxy composite samples, the RBSN matrix composite samples had lower relative thermal conductivities than the reference sample (ie. $K_C/K_M < 1$). The actual thermal conductivities of the HBN samples were found to be 6.94, 9.55, 8.74, and 7.30 W/m·°K, in order of highest to lowest HBN volume fraction. The lone diamond sample had a thermal conductivity of 15.71 W/m·°K. One interesting note regarding this data is that the reference sample was found to have a thermal conductivity of 17.11 W/m·°K, which is almost twice the normally observed thermal conductivity of RBSN.

The RBSN results were disappointing, since the acoustic properties of HBN match up very well with RBSN, as evidenced by the q, p, and η parameters on Table #3. Theoretically, the vast majority of the phonons should be transmitted from the matrix into the HBN particles (and back again). One explanation for the poor results is poor contact between the matrix material and the dispersed particles. This may be a distinct possibility considering the relatively high processing temperatures associated with nitriding the RBSN (1400°C). Since the thermal expansion coefficient of HBN in the radial direction is slightly larger than that of RBSN (3.4 and 2.9 * 10^{-6}/°K, respectively), microcracks may have formed between the RBSN and HBN during cooling of the samples. Microcracks around the HBN particles would severely reduce the thermal conductivity, due to the fact that the small spaces around the particles would act as pores in terms of the

thermal conductivity. As previously discussed, porosity significantly reduces the thermal conductivity of a material because air has a very low thermal conductivity and the small pockets of space around the particles would cause an extremely high boundary resistance which would prevent heat from being transferred to the filler particles. In the case of particulate composites, this problem is exacerbated by the fact that the majority of the void space is filled with a solid. This implies that the solid's heat capacity causes the void to act as a heat sink, and actually reduces the observed thermal diffusivity.

On the other hand, the thermal conductivity of the diamond sample was nearly identical to the reference sample, which is exactly what both theoretical models predict for samples with relatively low volume fraction. One additional note which must be made concerning the HBN samples is that they were all relatively thick (4 - 7 mm). This thickness may have had the effect of interfering with the incoming laser signal, and thus may have caused the observed diffusivity to be lower than the actual value. But this factor must be considered a relatively minor one, and is not a satisfactory explanation for the unexpectedly poor results.

Future RBSN research. Given the failure of this study to produce high thermal conductivity RBSN matrix composite material, possible improvements to the HBN sample processing and/or alternatives to HBN must be sought. In order to eliminate sample thickness as a major contributing factor, a new series of samples should be pressed while strictly limiting the thickness to about 2.5 mm. Also, in order to confirm the poor contact caused by thermal expansion coefficient mismatch, compression testing to find the modulus behavior and/or an acoustic loss analysis should be performed.

In the case that thinner samples do not improve the thermal conductivity significantly or that microcracking in the samples is confirmed, an alternative filler material to HBN must be found, or an improved HBN processing procedure must be developed. It may be possible to coat HBN particles with a material such as polysilazane, which is a RBSN forming agent which would bond the HBN particles to the matrix. If equation [9] is expressed in terms of material properties of RBSN, epoxy, and filler materials, the following equation results:

$$R_{BD} = 2 \cdot [(G_M \cdot \rho_M)^{0.5} + (G_D \cdot \rho_D)^{0.5}]^2 \cdot G_D^{0.5} \cdot \rho_D^{-1.5} / C_M \cdot G_M^2 \qquad [21]$$

Two plots of the boundary resistance vs. filler particle density and shear modulus relative to an epoxy matrix and a RBSN matrix are shown on Figure #7 and Figure #8. The plots clearly show that increasing density and decreasing shear modulus of the filler particles reduce the boundary resistance between the matrix material and the filler particles. If HBN proves to be unusable as a filler material, future studies of RBSN composites must focus on the selection of the filler material. It can be inferred from the above results infer that 4 factors are crucial in the selection of a filler material: 1) high density, 2) low shear modulus, 3) high thermal conductivity, and 4) good thermal expansion coefficient match with RBSN.

Figure 3

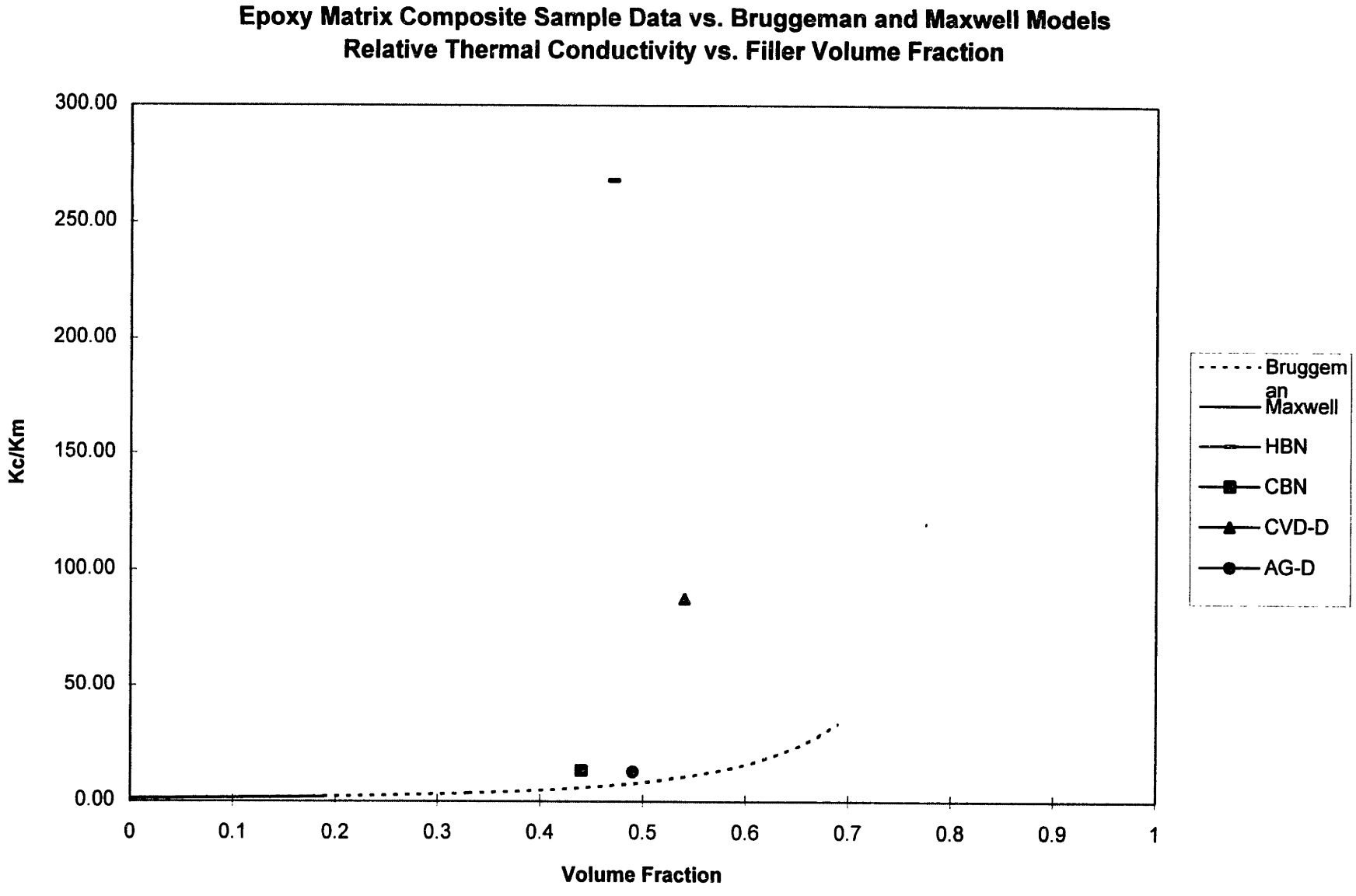
Epoxy Matrix Composite Sample Data vs. Bruggeman and Maxwell Models
Relative Thermal Conductivity vs. Filler Volume Fraction
Kc/Km
300.00
250.00
200.00
150.00
100.00
50.00
0.00
0
0.1
0.2
0.3
0.4
0.5
0.6
0.7
0.8
0.9
1
Volume Fraction
Bruggeman
Maxwell
HBN
CBN
CVD-D
AG-D

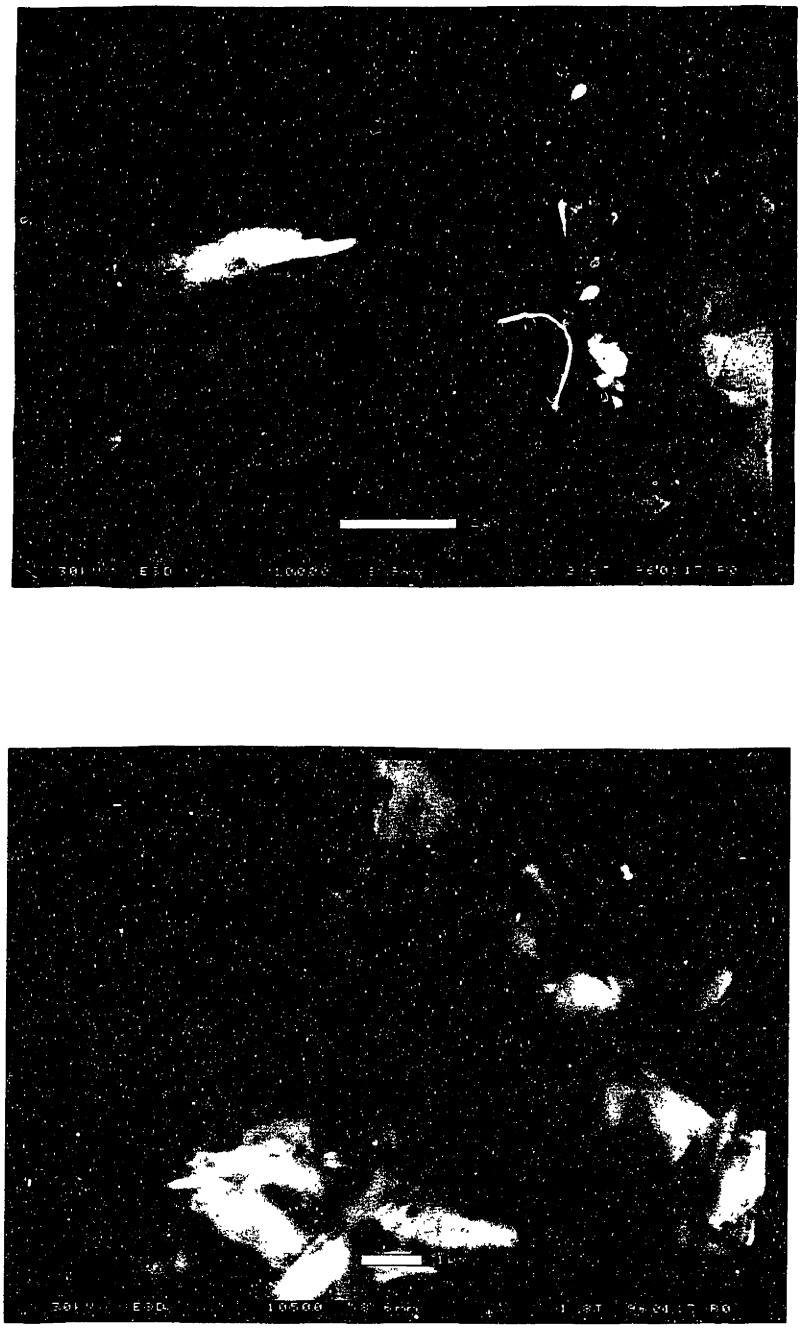

Figure #6: SEM micrographs of radial (upper) and axial (lower) view of HBN-epoxy composite sample

Table #1: Boundary Resistance Calculations for Epoxy Matrix Composite Samples

Additive	Density (kg/m^3)	C_P (J/kg*K)	G ($kg/m*sec^2$)	v (m/sec)	Z (kg/m^2*S)	q (fraction)	p (probability)	N (probability)	R_{BD} (K/m^2*W)
HBN	2300	700	2.29E+10	3155	7.26E+06	4.37E-02	0.448	1.96E-02	1.06E-07
CBN	3500	700	2.29E+10	2558	8.95E+06	6.66E-02	0.382	2.54E-02	8.16E-08
CVD-D	3520	509	5.76E+11	12792	4.50E+07	2.66E-03	0.091	2.42E-04	8.58E-06
GE-D	3520	509	5.76E+11	12792	4.50E+07	2.66E-03	0.091	2.42E-04	8.58E-06
Epoxy	1148	1800	1.00E+09	933	1.07E+06				

Table #2: Relative Thermal Conductivity and Kapitza Radius Calculations for Epoxy Matrix Composite Samples

Additive	Diffusivity (m^2/sec)	Mass (g)	Volume (cm^3)	$Density_{Comp}$ (kg/m^3)	f (fraction)	$Density*C_P$ (J/m^3*K)	$(D*C_P)_{Comp}$ (J/m^3*K)	K_M (W/m*K)	K_C (W/m*K)	K_C/K_M (ratio)	a_K (m)
HBN	3.32E-05	0.2847	0.1682	1693	0.473	1.61E+06	1.85E+06		61.44	267.86	2.43E-08
CBN	1.33E-06	0.2925	0.1337	2188	0.442	2.45E+06	2.24E+06		2.97	12.96	1.87E-08
CVD-D	1.05E-05	0.5303	0.2177	2436	0.543	1.79E+06	1.92E+06		20.13	87.76	1.97E-06
GE-D	1.47E-06	0.4907	0.2158	2274	0.475	1.79E+06	1.94E+06		2.85	12.41	1.97E-06
Epoxy	1.11E-07	0.2520	0.2195	1148	1.000	2.07E+06		0.229			

Table #3: Boundary Resistance Calculations for RBSN Matrix Composite Samples

Material	Density (kg/m^3)	C_P (J/kg*K)	G ($kg/m*sec^2$)	v (m/sec)	Z (kg/m^2*S)	q (fraction)	p (probability)	N (probability)	R_{BD} (K/m^2*W)
HBN	2300	700	2.29E+10	3155	7.26E+06	1.000	0.813	0.813	3.358E-10
CVD-D	3520	509	5.76E+11	12792	4.50E+07	0.154	0.822	0.127	2.157E-09
RBSN	2580	800	1.30E+11	7098	1.83E+07				

Table #4: Relative Thermal Conductivity and Kapitza Radius Calculations
for RBSN Matrix Composite Samples

Additive (volume f)	Density (kg/m^3)	C_P (J/kg*K)	Density*C_P (J/m^3*K)	Diffusivity (m^2/sec)	Mass (g)	$V.F._{Additive}$ (fraction)	$(D*C_P)_{Comp}$ (J/m^3*K)	K_M (W/m*K)	K_C (W/m*K)	K_C/K_M (ratio)	a_K (m)
HBN - 70				3.98E-06	1.6764	0.705	1.74E+06		6.94	0.41	5.75E-09
HBN - 60				5.32E-06	0.8457	0.593	1.79E+06		9.55	0.56	5.75E-09
HBN - 50				4.82E-06	1.2076	0.553	1.81E+06		8.74	0.51	5.75E-09
HBN - 30				3.79E-06	1.2988	0.304	1.93E+06		7.30	0.43	5.75E-09
CVD - 20				7.82E-06	0.6516	0.200	2.01E+06		15.71	0.92	3.69E-08
RBSN				8.29E-06	0.4241	0.000	2.06E+06	17.111			

Material			
HBN	2300	700	1.61E+06
CVD-D	3520	509	1.79E+06
RBSN	2580	800	2.06E+06

Table #5: Percent Conversion and Volume Fraction Data for RBSN Matrix Composite Samples

Sample	Si weight % (percent)	Mass (pre-nit) (g)	Mass (post-Nit) (g)	% Conv. (w) (percent)	% Conv. (XRD) (percent)	Vol. Fraction (fraction)
RBSN Ref	100.0	0.2672	0.4380	96.1	97.7	0.000
HBN - 70	23.0	1.4826	1.6764	85.4	96.4	0.705
HBN - 60	31.6	0.6982	0.8457	100.5	97.9	0.593
HBN - 50	36.0	0.9910	1.2076	91.2	95.7	0.553
HBN - 30	61.5	0.9453	1.2988	91.5	97.2	0.304
CVD-D - 20	64.1	0.4612	0.6516	96.9	99.0	0.200

Figure #7

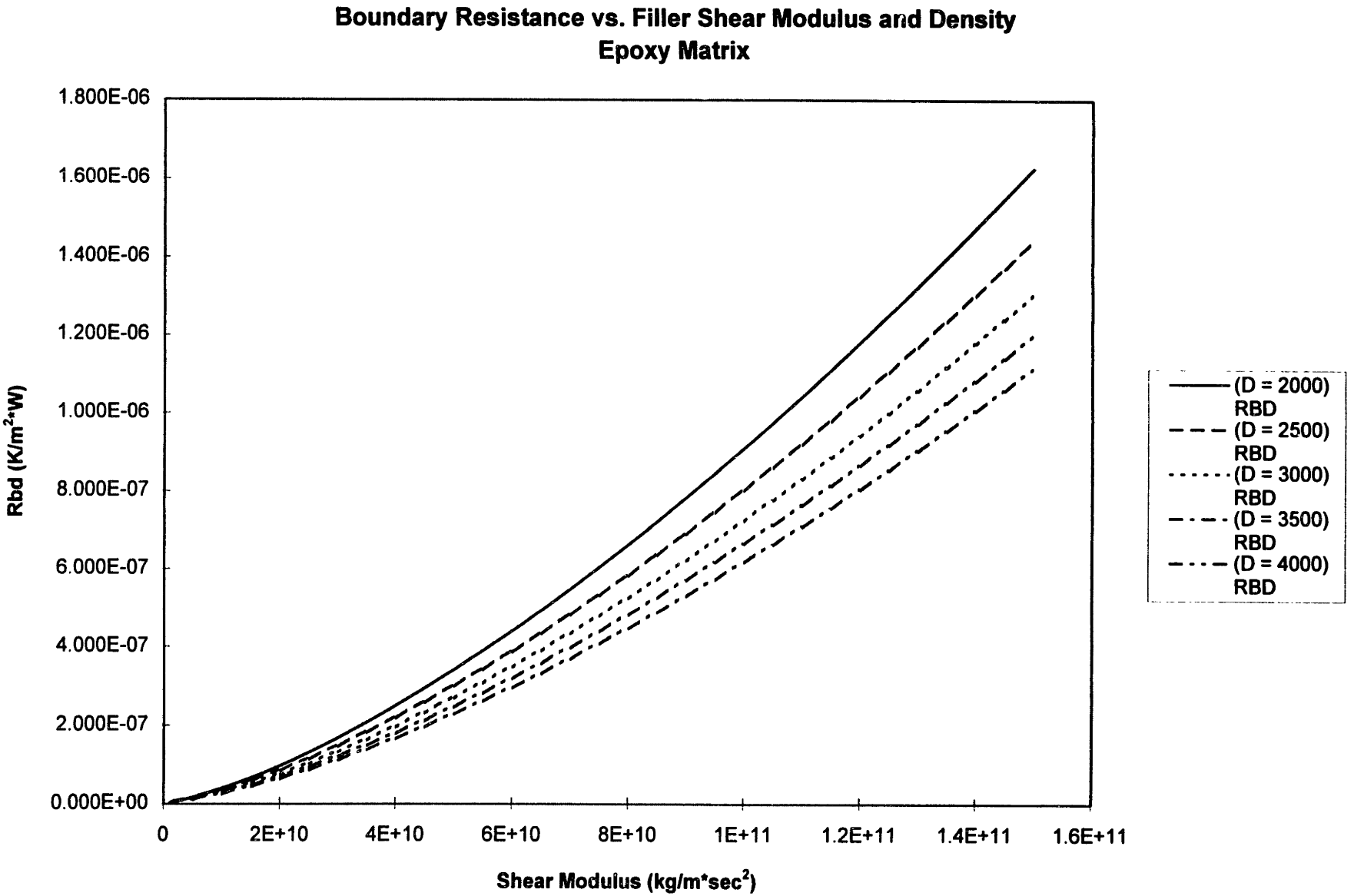
Boundary Resistance vs. Filler Shear Modulus and Density
Epoxy Matrix
Rbd (K/m²*W)
1.800E-06
1.600E-06
1.400E-06
1.200E-06
1.000E-06
8.000E-07
6.000E-07
4.000E-07
2.000E-07
0.000E+00
0
2E+10
4E+10
6E+10
8E+10
1E+11
1.2E+11
1.4E+11
1.6E+11
Shear Modulus (kg/m*sec²)
(D = 2000) RBD
(D = 2500) RBD
(D = 3000) RBD
(D = 3500) RBD
(D = 4000) RBD

Figure #8

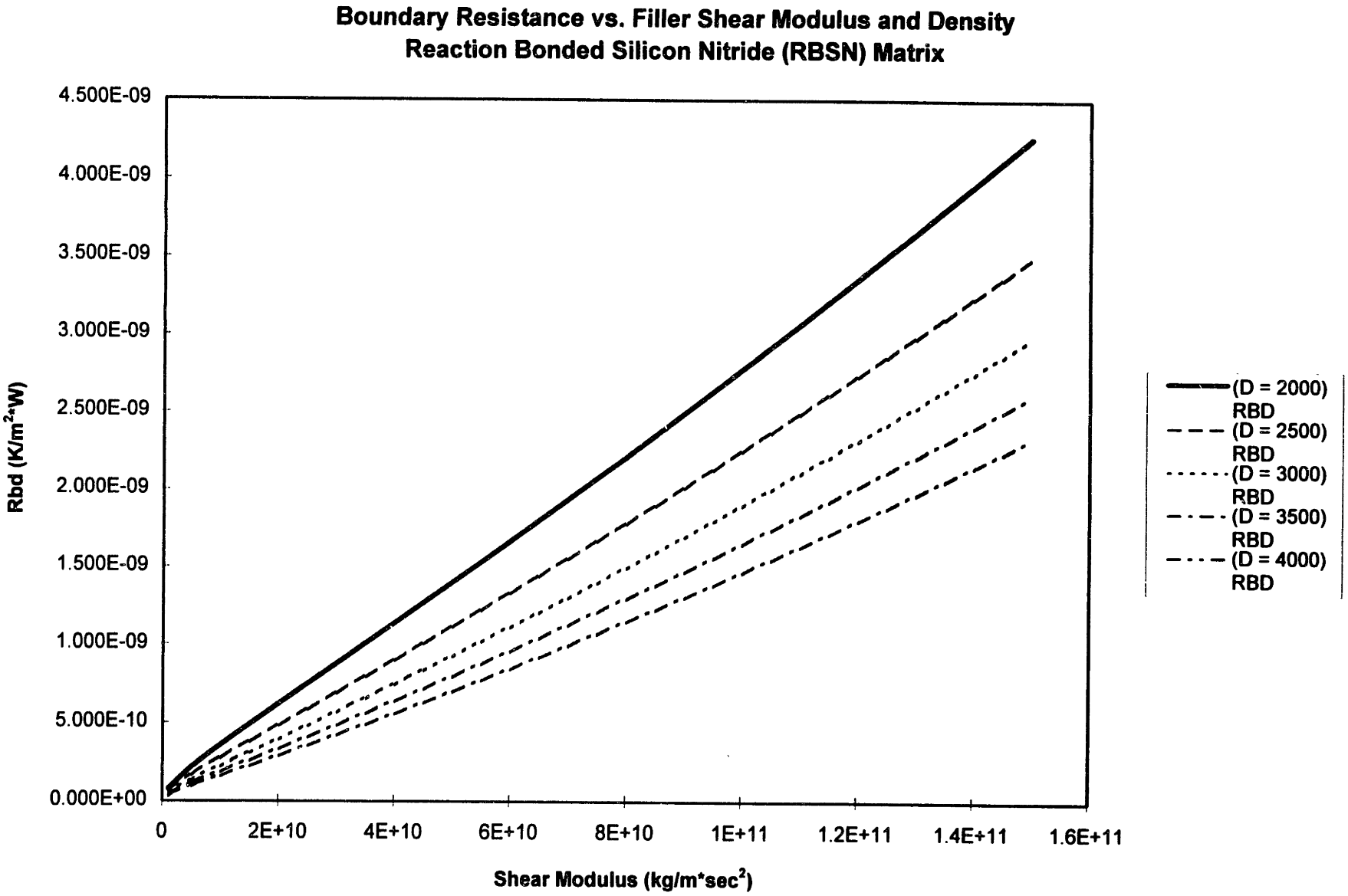
Boundary Resistance vs. Filler Shear Modulus and Density
Reaction Bonded Silicon Nitride (RBSN) Matrix
Rbd (K/m²*W)
4.500E-09
4.000E-09
3.500E-09
3.000E-09
2.500E-09
2.000E-09
1.500E-09
1.000E-09
5.000E-10
0.000E+00
0
2E+10
4E+10
6E+10
8E+10
1E+11
1.2E+11
1.4E+11
1.6E+11
Shear Modulus (kg/m*sec²)
(D = 2000) RBD
(D = 2500) RBD
(D = 3000) RBD
(D = 3500) RBD
(D = 4000) RBD

CONCLUSION

In this study, high thermal conductivity samples were created using epoxy as a matrix material with filler materials of HBN and CVD-D. The epoxy results seem to indicate that high thermal conductivity particulate composite materials can be produced. On the other hand, the combination of HBN particles in a RBSN matrix failed to provide high thermal conductivity material. Microcrack testing in the form of compression testing or acoustic loss analysis should be performed on the RBSN samples used in this study. Also, thinner RBSN composite samples must be pressed and new diffusivity measurements taken to confirm that HBN requires special processing (ie. bonding material, etc.) if it is to be used in RBSN matrix composites. If HBN is ruled out as a candidate material, an alternative high thermal conductivity material such as diamond should be studied which matches RBSN's thermal expansion and acoustic properties.

REFERENCES

[1]Haggerty, J. S., "Synthesis and Properties of Reaction Bonded Silicon Nitride Made From High Purity Silicon Powders", *Silicon-Based Structural Ceramics*, Vol. 42, pp.29-45, 1993.

[2]Riley, F. L., "Reaction Bonded Silicon Nitride", *Materials Science Forum*, Vol. 47, pp. 70-83, 1989.

[3]Slack, G. A., "Nonmetallic Crystals with High Thermal Conductivity", *Journal of Physics and Chemical Solids*, Vol. 34, pp.321-335, 1973.

[4]Berman, R., *Thermal Conduction in Solids*, Clarendon Press, Oxford, U.K., 1976.

[5]Swartz, E. T., and Pohl, R. O., "Thermal Boundary Resistance", *Reviews of Modern Physics*, Vol. 61, No. 3, pp. 605-668, 1989.

[6]Mazo, R. M., "Theoretical Studies on Low Temperature Phenomena", Ph.D. thesis, Yale University, 1955.

[7]Swartz, E. T., and Pohl, R. O., "Thermal Resistance at Interfaces", *Applied Physics Letters*, Vol. 51, p. 200, 1987.

[8]Auld, B. A., *Acoustic Fields and Waves in Solids*, Vol. I, 124, Wiley, New York, 1973.

[9]Weis, O., "Phonon Radiation Across Solid/Solid Interfaces Within the Acoustic Mismatch Model", *Nonequilibrium Phonons in Nonmetallic Crystals*, p. 1, 1986.

[10]Hasselman, D. P. H., "The Effect of Particle Size on the Thermal Conductivity of ZnS/Diamond Composites", *Acta Metallurgical Materials*, Vol. 40, No. 1, pp. 123-129, 1992.

[11]Hasselman, D. P. H., and Johnson, L. F., "Effective Thermal Conductivity of Composites with Interfacial Thermal Barrier Resistance", *Journal of Composite Materials*, Vol. 21, pp. 508-515, 1987.

[12]Benveniste, Y., "Effective Thermal Conductivity of Composites with a Thermal Contact Resistance Between the Constituents: Nondilute Case", *Journal of Applied Physics*, Vol. 61, No. 8, pp. 2840-2843, 1987.

[13]Kingery, W. D., Bowen, H. K., and Uhlmann, D. R., *Introduction to Ceramics*, John Wiley and Sons, New York.

[14]Beecher, S. C., Dinwiddle, R. B., and Lowden, R. A., "The Thermal Conductivity of Carbon Coated Silicon Carbide Fibers Embedded in a Silicon Carbide Matrix", *Thermal Conductivity*, Vol. 22, pp. 324-334, 1994.

[15]Nitrides, Metals, and Ceramics Information Center, *Engineering Property Data on Selected Ceramics, Volume I*, Battele Columbus Laboratories, Columbus, Ohio.

[16]*CRC Handbook of Chemistry and Physics*, CRC Press, Inc., Boca Raton, FL, 1985.

[17]Kretzschmar, K., and Hoffman, K. W., "Effect of Heat Capacity Changes on the DSC Base Line at the Curing of Epoxy Resins", *Thermochimica Acta*, Vol. 151, pp. 233-240, 1989.

[18]Levita, G., "Effect of Cure Temperature on the Mechanical Properties of ATBN/Epoxy Blends", *Polymer*, Vol. 26, pp. 1112-1113.

[19]"Standard Test Method for Water Absorption, Bulk Density, Apparent Porosity, and Apparent Specific Gravity of Fired Whiteware Products", ASTM, Standard C - 373, 1972.

THESIS PROCESSING SLIP

FIXED FIELD ill _____ name _____

index _____ biblio _____

▶ COPIES: (Archives) Aero Dewey Eng Hum

Lindgren Music Rotch Science

TITLE VARIES ▶☐ _____

_____

_____

NAME VARIES: ▶☒ See degree book

_____

IMPRINT (COPYRIGHT) _____

▶ COLLATION: 40 ℓ

_____

▶ ADD. DEGREE: _____ ▶ DEPT.: _____

SUPERVISORS: _____

_____

_____ _____

_____ _____

_____ _____

_____ _____

_____ _____

_____ _____

_____ _____

NOTES:

cat'r: date:

▶ DEPT: Mat Sci & E page: ▶ F11

▶ YEAR: 1996 ▶ DEGREE: B.S.

▶ NAME: ~~Ste~~ STEPHENS, Clifford

_____